 doi:10.20944/preprints202210.0133.v1

Article

Efficiency of Adsorption and Photodegradation of Composite TiO2/Fe2O3 and Industrial Waste in Cyanide Removal

Blanca Margarita Amaro-Medina[1], Antonia Martinez-Luevanos[1,*], Ma. de Jesus Soria-Aguilar[2], Marco Antonio Sanchez-Castillo[3], Sofia Estrada-Flores[1] and Francisco Raul Carrillo-Pedroza[2,*]

[1] Facultad de Ciencias Químicas, Universidad Autónoma de Coahuila, Ing. J. Cárdenas Valdez S/N, República, 25280 Saltillo, Coahuila, Mexico; aml15902@uadec.edu.mx; sofiaestrada@uadec.edu.mx; bamaro@uadec.edu.mx

[2] Facultad de Metalurgia, Universidad Autónoma de Coahuila, Carretera 57 Km 5, 25710 Monclova, Coahuila, Mexico; ma.soria@uadec.edu.mx; raul.carrillo@uadec.edu.mx

[2] Facultad de Ciencias Químicas, Universidad Autónoma de San Luis Potosí, Manuel Nava 6, San Luis Potosí, S.L.P. 78210, Mexico; masanchez@uaslp.mx

* Correspondence: FRCP: raul.carrillo@uadec.edu.mx; AML: aml15902@uadec.edu.mx

Abstract: This research is mainly focused on the evaluation of TiO_2/Fe_2O_3 composite and two industrial types of waste (kaolin (Clay-K) and a blast furnace sludge (BFS)) as adsorbent materials of cyanide and as photocatalysts. First, adsorption tests were performed in the absence of light. During photodegradation experiments, the effect of the type of irradiation (ultraviolet (UV) light), visible light and natural sunlight), irradiation time, the type of photocatalyst, as well as irradiance in case of natural sunlight use, were investigated. Adsorption results indicate that Clay-K and TiO_2/Fe_2O_3 materials adsorb approximately twice as much cyanide compared to the BFS sample, which only adsorbs 33.3% (124.87 mg/g); this is due to its smaller specific surface area (5.69 m^2/g) compared to that of the other two materials (Clay-K and TiO_2/Fe_2O_3 (14.93 m^2/g and 66.59 m^2/g, respectively). The results obtained from the study of photodegradation of cyanide under UV irradiation, indicate that Clay-K and BFS samples photodegrade cyanide by 96.44% and 92.66%, respectively. On the other hand, using UV irradiation plus solar irradiation and visible plus solar irradiation, the best photocatalyst was the TiO_2/Fe_2O_3, with 98.66% photodegradation. The use of natural sunlight (irradiance of 600 to 800 W/m^2) of a NaCN solution of 750 mg/L, the BFS material was the most efficient to photodegrade cyanide, obtaining 97% in two hours and 87% in just 30 minutes of irradiation.

Keywords: cyanidation wastewater; cyanide; photodegradation; adsorption; clay; blast furnace sludge

1. Introduction

Cyanidation is the gold and silver extraction process that has been used for a century in metallurgical operations of precious metals extraction around the world, due to its high efficiency of extraction using a wide variety of ores and concentrates, in addition to representing a low cost and high stability [1,2]. Gold extraction takes places due to the formation of the cyanide complex, according to Elsner's reaction [3]:

$$4\,Au + 8\,CN^- + O_2 + 2\,H_2O \rightarrow 4\,Au(CN)_2^- + 4\,OH^-$$

As a result of the cyanidation process, various soluble compounds, such as free cyanide and metal complexes, coexist, generating cyanide-containing effluents in concentrations between 40 and 600 mg/L [2,4]. The main problem associated with these effluents is short-term environmental damage, for example, if an accident occurs during operation, as well as spills or filtration into waterways. In the long term, environmental damage can also be caused, due to the formation of acid drains or mobility of heavy metals contained in the waste generated from the cyanidation process [5]. For cyanide, the limit of global

Preprints (www.preprints.org) | NOT PEER-REVIEWED | Posted: 11 October 2022 doi:10.20944/preprints202210.0133.v1

mean concentration that has been set for surface water is 2 µg/L and for treated groundwater is 8 µg/L [6]. The lethal dose in humans, orally or inhaled, is approximately 1 to 3 mg of free cyanide per kg of body mass [7].

There are several methods for degradation and removal of cyanide. Adsorption is one of the methods used for removing cyanide from aqueous solutions, since this process is easy to operate and control, it also presents a simple design, and different types of adsorbent materials can be used [8,9]. Some of the materials used for cyanide adsorption are activated carbon[10,11], iron-modified zeolites [9,12], zinc oxide [13], chitosan-polyacrylamide [14], pistachio shell residues [15] and coke powder [16].

Some adsorbent materials may exhibit photocatalytic activity, a property that has also been used for the oxidation of cyanide. Therefore, knowing the adsorption capacity of a photocatalyst material is of great importance in the overall efficiency of the heterogeneous catalysis process since species must be adsorbed in the first instance to begin the redox reaction [17].

In heterogeneous photocatalysis, the catalyst is activated by light absorption and a photo-generation of electron-hole pairs occurs on the surface of the material. The excited electrons are transferred to the reducible species, whereas the catalyst accepts the electrons of the oxidizable species occupying the gaps, such that the flow of electrons is null, and it does not alter or affect the catalyst [18]. This process is used when the species to be treated does not capture photons by itself, so, when adding the catalyst, an energy change originates and reactive species such as the hydroxyl radical OH* are generated, which is an oxidizing species of great importance during advanced oxidation processes [19].

TiO_2 is the most used semiconductor in photocatalysis, because it is a chemically and biologically inert compound, in addition to presenting stability to chemical and photochemical corrosion, it has a gap of 3.2 eV and can be excited with ultraviolet light, at a wavelength less than 387 nm. Photocatalysis with titanium oxide is of great interest because it can be reused without deterioration in its photoactivity, and it does not present toxicity, it also has great stability under irradiation and it is inexpensive [20].

The reactions shown below are those carried out in the oxidation of cyanide using TiO_2 and irradiation [20]:

$$CN^- + 2H^+ + 2OH^- \rightarrow CNO^- + 2H_2O$$
$$CNO^- + 4O_2 + 2OH^- + 3H_2O \rightarrow CO_3^{2-} + NO_3^- + 4H_2O_2$$

Pavas et al. conducted several experiments using TiO_2 as a catalyst and H_2O_2 as an oxidizing agent, with a cyanide concentration of 400 ppm, using a tubular photo-reactor of 90-150 W with a recirculation time of 2 hours. The percentage of cyanide reduction at 2 hours, using UV/H_2O_2 was 57%, with UV/TiO_2/H_2O_2 of 65.50%, the latter system and the addition ofO_2 achieved 65.50%[21].

Quispe et al. performed cyanide removal with a UV/H_2O_2 and TiO_2 system, using a photocatalytic reactor. In the experiments carried out, they observed that as the concentration of hydrogen peroxide increased, the elimination of cyanide increased, as well; the UV-irradiated TiO_2 system led to the degradation of up to 99.6% cyanide, as well as a decrease in pH to 10.47 in 1 hour of exposure. Using the combination TiO_2-H_2O_2-UV a degradation of 99.9% of cyanide was obtained and the pH decreased to 9.54 after 1 hour of reaction[22].

Viña et al. studied the degradation of cyanides and thiocyanates simultaneously, present in wastewater, with simulated sunlight and UV light, comparing their efficiency with TiO_2. They obtained a 50% conversion of cyanide at 2 hours of UV irradiation[23].

Caicedo et al. investigated the adsorption and photocatalysis of ferricyanide, using TiO_2 (P25) as a photocatalyst. The irradiation of the solution was carried out with a lamp of 300 W, with a wavelength of 300 nm; a flow of 4 L/min H_2O_2 (pH 13) was added. A degradation of 83% was achieved in one hour[24].

Preprints (www.preprints.org) | NOT PEER-REVIEWED | Posted: 11 October 2022 doi:10.20944/preprints202210.0133.v1

Iron oxides have also been evaluated as photocatalysts, and they have exhibited a considerable photocatalytic activity. Being these derivatives of a natural mineral, not only are they stable but also inexpensive, so they are commonly used in ozonation [15].

Seung-Mok et al. reported that Fe(VI) has a great potential for oxidation from CN^- to CNO^-, which is 1000 times less toxic. Fe(VI) decomplexes metallic cyanide, first, and then degrades to free cyanide [25]:

$$Fe(VI) + CN^- \rightarrow Fe(III) + CNO^-$$
$$CN^- + 2OH^- + 2h_{vb}^+ \xrightarrow{TiO_2+UV} CNO^- + H_2O$$
$$CNO^- + 2H_2O \rightarrow NH_4^+ + CO_3^{2-}$$

Seung-Mok et al. also reported the performed CN- oxidation, as well as copper or nickel removal from cyanide solutions, using Fe(VI). The initial cyanide concentration dropped from 1 mmol/L to 0.002 mmol/L and copper was almost completely removed at pH=13 [25].

Yngard et al. conducted a kinetic study on the reaction of Fe(VI) with a zinc cyanide complex, at pH range 9 to 11. As pH increased speed constant decreased. They also studied the effect of temperature at a range 15 to 45°C, on cyanide oxidation at pH=9; an activation energy of 45.7 KJ/mol was obtained. This group of researchers conducted experiments on a real sample of rinse water, in which conversion of cyanide was complete to cyanate [26].

Eskandari et al. conducted an experiment of adsorption and cyanide photo-degradation with UV light. In this study, two different materials based on TiO_2 and Fe_2O_3 (TiO_2/Fe_2O_3/Zeolite and TiO_2/Fe_2O_3/PAC) were used; they also used H_2O_2 as an oxidant. With the first catalyst, a degradation rate of 91% was achieved, whereas for the second it was 97%. With the use of the catalyst TiO_2/Fe_2O_3/PAC a better performance was obtained due to its high surface area of 254.64 m^2/g, compared to the area of the catalyst TiO_2/Fe_2O_3/Zeolite of 112.69 m^2/g [27].

On the other hand, a material of interest is kaolin, which is an aluminosilicate that contains kaolinite, ($Al_2O_3{\cdot}2SiO_2{\cdot}2H_2O$), with iron and titanium impurities in the form of oxides, oxyhydroxides and carbonates [28]. These impurities can absorb light and thus produce the formation of reactive species, with hydroxyl radical (OH*) being the main one [29]. Behnamfard, et al. investigated the removal of free cyanide (CN^-) in aqueous solutions by adsorption, using kaolin. They obtained adsorptions of 2.5, 3, and 8 mg/g using crude, calcined and kaolin treated with sulfuric acid, respectively [9].

The aim of this work is to investigate the efficiency of the composite TiO_2/Fe_2O_3 synthesized by mechanosynthesis, as well as of two industrial residues, called Clay-K (contains kaolinite, quartz, TiO_2, and Fe_2O_3) and BFS (contains kaolinite, quartz, graphite, and various types of iron oxides), as cyanide adsorbent materials and as photocatalysts of cyanide oxidation in aqueous solutions. The evaluation of these materials as photocatalysts of cyanide photo-oxidation was carried out under irradiation with visible light, UV light, and with natural sunlight. By using solar energy as a lighting source for cyanide removal, operating costs can be reduced as effluent treatment simplified.

2. Materials and Methods

2.1. Adsorbent and photocatalytic materials.

For the removal of cyanide by adsorption and photodegradation of aqueous solutions, three materials were selected. Two of these materials are industrial waste containing silica (quartz), kaolinite, iron and titanium oxides (Clay-K) and various types of iron oxides and graphite (BFS); the other material is the composite TiO_2/Fe_2O_3, which was synthesized by the method of mechanosynthesis.

Obtaining and preparation of Clay-K and BFS materials. The material called in this work "Clay-K" is an industrial waste, which was sieved, and the different size fractions were

Preprints (www.preprints.org) | NOT PEER-REVIEWED | Posted: 11 October 2022 doi:10.20944/preprints202210.0133.v1

collected; for this study, the sample with particle size fraction -75/+45 μm was selected. Its main mineralogical composition is quartz and kaolinite; its chemical composition is mainly silicon and aluminum oxides, it also contains 1.27% and 0.1% of Fe_2O_3 and TiO_2, respectively. The material called "BFS" comes from the metallurgical industry, its main mineralogical composition is quartz, kaolinite and graphite, its chemical composition is mainly based on silicon and aluminum oxides and carbon, it also contains various types of iron oxides in smaller quantities. This material was used in adsorption and photodegradation tests as received.

Synthesis of the composition TiO_2/Fe_2O_3. TiO_2/Fe_2O_3 composite was obtained by mechanosynthesis, 0.1 mol of TiO_2 phase anatase, previously obtained by the sol-gel method, according to a procedure reported by Estrada-Flores, et al., was placed into a container of zirconia of 200 mL, thence it was mixed with 2% in mol of Fe_2O_3 [30]. The container was placed in a Fritsch planetary ball mill (model Pulverisette 6) and the mixture was left in stirring for 20 minutes at 250 rpm. After this time, a red powder was obtained, which was subjected to a thermal treatment at 450 °C, using a heating rate of 2°C/min. The ball load ratio was 1:10. Figure 1 presents a diagram of this synthesis procedure.

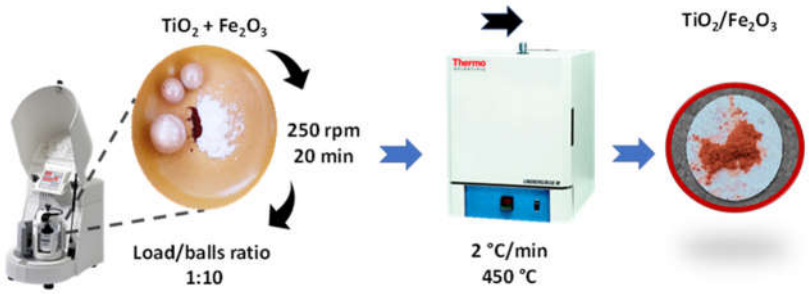

Figure 1. Diagram showing the shynthesis of TiO_2/Fe_2O_3 composite by the mechanosynthesis method.

2.2. Characterization.

Chemical and structural characterization of samples was carried out by infrared spectroscopy using a Thermo Scientific equipment, model Nicolet iS10; infrared spectra were acquired in the range of 4000 cm^{-1} to 400 cm^{-1}, with a resolution of 4 cm^{-1} and the attenuated reflectance accessory (ATR) was used. X-ray diffractograms were obtained using a Rigaku equipment, model Ultima IV, with D/teX detector, with a speed of passage of 0.05 °. Clay-K and BFS samples were characterized by optical microscopy, whereas the TiO_2/Fe_2O_3 sample was characterized by scanning electron microscopy (SEM), a JEOL microscope Model JSM-7800F was used. Absorption spectra of the sample were obtained using a Perkin Elmer equipment, Lambda 35 model with integration sphere; Spectralon® white diffuse reflectance standard was used for calibration. The specific surface area of the three samples was determined by the BET Theory (Brunauer – Emmett – Teller) using the data obtained with the Quantachrome Instrument l equipment and using nitrogen gas as an adsorbent. The isoelectric point (pH_{IEP}) of the TiO_2/Fe_2O_3 sample was determined through the measurement of zeta potential as a function of pH, for which an Anton Paar equipment, Litesizer 500 model, was used. Aqueous suspensions of Clay-K and BFS samples were prepared at a concentration of 1 mg/ml and the pH was adjusted to 7 and the ionic strength to 1 mM with potassium chloride (KCl, Sigma-Aldrich, 99%).

2.3. Preparation of NaCN solutions.

Two liters of deionized water were added in a two-liter glass and sodium hydroxide (NaOH, Sigma-Aldrich, 98%) was added until reaching a pH =11; pH was measured with a glass electrode (Orion), connected to a potentiometer (Orion, model 710A); Electrode-potentiometer system was previously calibrated with pH buffer solutions 4, 7, and 10 (J.T

Preprints (www.preprints.org) | NOT PEER-REVIEWED | Posted: 11 October 2022 doi:10.20944/preprints202210.0133.v1

Baker). This alkaline solution was used to prepare one liter of stock sodium cyanide solution (NaCN, Sigma-Aldrich, 97%) of 1000 mg/L, for which 1.03 g of NaCN was added in a volumetric one-liter flask and the alkaline solution was added until calibrated. From this stock, solutions of 50, 100, 250 and 750 mg/L of NaCN were prepared.

2.4. Adsorption experiments.

Effect of the type and initial NaCN concentration A certain predefined amount of TiO_2/Fe_2O_3, Clay-K, and BFS materials was weighed and added to 15 ml glass tubes, coated with aluminium foil, containing 10 ml of aqueous NaCN solution, at a predefined concentration (250 mg/L and 750 mg/L). The material was then dispersed into the cyanide solution using ultrasound for one minute; subsequently, the tubes with the dispersions were kept for 2 hours in an incubator, at 25 °C ± 1°C and in the absence of light. After this time, the solid/liquid separation was performed by centrifugation at 8000 rpm for 5 minutes and the clarified liquid was collected for the quantification of cyanide by means of the titration technique with silver nitrate solution ($AgNO_3$, Sigma-Aldrich, 99%) and using potassium iodide as an indicator (KI, Sigma-Aldrich, 99%).

Adsorption kinetics. These tests were performed in the absence of light, at an initial cyanide concentration of 750 mg/L; a concentration of adsorbent material (TiO_2/Fe_2O_3, Clay-K, and BFS) of 2 g/L was used. At a previously pre-established contact time, the solid-liquid separation was carried out by centrifugation at 8000 rpm for 5 minutes; the clarified liquid was collected and used for the quantification of remaining cyanide in the titration solution. Temperature remained constant at 25 °C ± 1°C.

2.5. Photodegradation Experiments.

Effect of the type of catalyst and the type of irradiation. 20 mg of each material were weighed, and added to 15 ml glass tubes, coated with aluminum foil, containing 10 ml of aqueous solution of NaCN, at a concentration of 750 ppm. The material was then briefly dispersed into the cyanide solution using ultrasound for one minute; subsequently, the tubes with the dispersions were kept for 2 hours in an incubator, at 25 °C (in the absence of light). After this time, the samples were moved to a system for photo-oxidation. This system consists of a 50 mL quartz tube, a bath of water recirculation to keep the temperature constant and a lamp with its source. The samples were irradiated for 2 hours with UV light, using a Mercury Lamp (Pen-Ray®, λ=254 nm, Irradiance= 4400 μW/cm^2, 300 V); then, the solid/liquid separation was performed by centrifugation at 8000 rpm for 5 minutes; the clarified liquid was collected to quantify cyanide present in the titration solution using a solution of $AgNO_3$ 0.01 M. This procedure was repeated, but with visible irradiation, for which a xenon lamp (Pen-Ray®, λ=467 nm, 300 V) and natural sunlight) were used.

Photodegradation kinetics. 20 mg of each of the three samples were weighed and added to 10 mL of NaCN, with an initial concentration of 750 mg/L, in 15 ml glass tubes, previously coated with aluminum foil. The material was then briefly dispersed in the ultrasound cyanide solution for one minute; subsequently, the scattered samples were kept for 2 hours in the incubator, at 25 °C and in the absence of light. The samples were then irradiated with natural sunlight. At a pre-established time, the solid-liquid separation was carried out by centrifugation at 8000 rpm for 5 minutes; the clarified liquid was collected to quantify cyanide present in the titration solution with a solution of $AgNO_3$. All photodegradation experiments were performed at 25 °C ± 1°C.

3. Results and discusion

3.1. Characterization

Preprints (www.preprints.org) | NOT PEER-REVIEWED | Posted: 11 October 2022 doi:10.20944/preprints202210.0133.v1

Optical micrographs of Clay-K and BFS samples Figure 2 (a) and (b) and micrograph (SEM) of the TiO_2/Fe_2O_3 composite (Figure c). Particles of iron oxides are observed in Figure 2a; agglomerated particles of Fe_2O_3 (red circle) and white particles of quartz or kaolinite (blue circle) are observed. In Figure 2c is observed that the TiO_2/Fe_2O_3 sample contains porous, and it is formed by nanoparticles. Average zeta potential values for BFS and Clay-K samples are shown in Table 5.1. The zeta potential of Clay-K is -29.9 mV at pH 7 whereas that of BFS is 27.13 mV; the surface charge of both materials is likely to be negative at pH 11. Figure 1d presents the variation of the zeta potential of the TiO_2/Fe_2O_3 sample as a function of pH, extrapolation yields the value of the isoelectric point of 6.9 (pH_{IEP}); this implies that the surface of this sample has a positive charge at pH values lower than 6.9, whereas its surface is negatively charged at pH values higher than 6.9. It is important to note that cyanide solutions are usually prepared at pH equal to or close to 11, so it must be considered that the surface of clay and TiO_2/Fe_2O_3 materials will have a negative surface charge at this pH value.

On the other hand, the results of the characterization by the BET technique indicate that the values of the specific surface area (A_{BET}) of Clay-K, BFS, and TiO_2/Fe_2O_3 samples are 14.93 m_2/g, 5.69 m^2/g and 66.59 m^2/g, respectively.

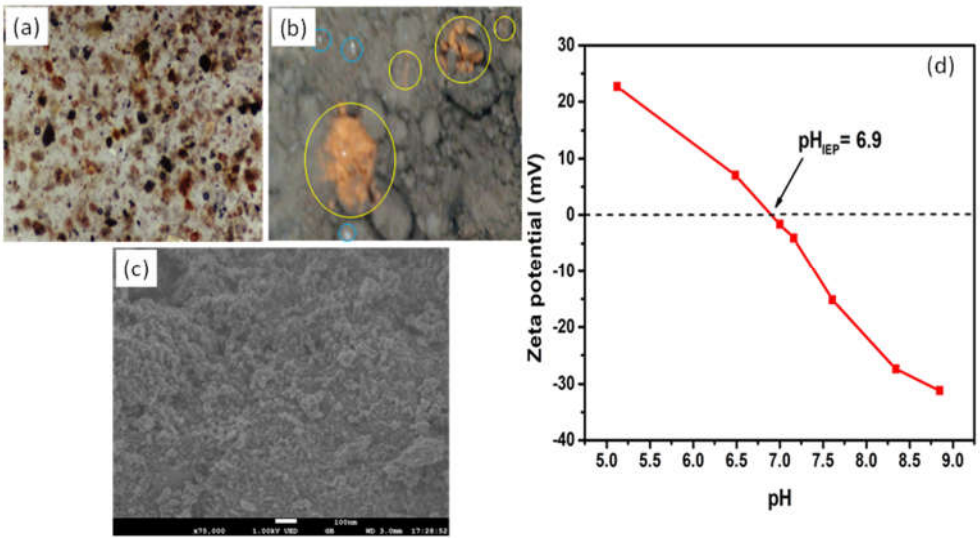

Figure 2. Optical micrographs at 500 X of Clay-K and BFS samples (a and b, respectively) and micrograph (SEM) at 75000X of the TiO_2/Fe_2O_3 sample (c). Zeta potential of the TiO_2/Fe_2O_3 sample as a function of pH (d).

Table 1. Zeta potential, pH_{IEP} and specific surface area (A_{BET}) of Clay-K, BFS, and TiO_2/Fe_2O_3 materials.

Material	Average zeta potential (mV)[a]	pH_{IEP}	A_{BET} (m^2/g)
TiO_2/Fe_2O_3	-1.60	6.90	66.59
Clay-K	-29.90	-	14.93
BFS	27.13	-	5.69

[a] = measured value at pH 7

The chemical and structural characterization of TiO_2/Fe_2O_3, Clay-K, and BFS samples was performed by infrared spectroscopy and X-ray diffraction. Figure 3 shows the infrared spectra of each of the samples. The infrared spectrum of the BFS sample presents absorption bands characteristic of the C-H bond stretching, which are at 2900 cm^{-1} and the vibrations of the C-H and C=O bond at 1560 cm^{-1}, respectively; these absorption bands may be associated with the carbon present in this sample. An absorption band is also observed at 1030 cm^{-1} corresponding to the Si-O stretch, as well as other less intense

 doi:10.20944/preprints202210.0133.v1

absorption bands at lower values, which may be associated with the vibration of the M-O bond, where M represents Si and Fe, since this sample contains mainly silicon oxide and iron oxides in lesser amounts. The absorption bands at values less than 999 cm^{-1} that have been associated with the Si-O-Al bond of aluminosilicates are also observed.

On the other hand, the infrared spectrum of the Clay-K sample presents an absorption band in 999 cm^{-1}, which is associated with the stretching of the Si-O bond of siloxane; the absorption bands at values less than 999 cm^{-1} that have been associated with the Si-O-Al bond of aluminosilicates are also observed. At 3619 cm^{-1} an absorption band corresponding to the stretching of O-H from the water contained in the crystal structure of this clay is also present.

The FTIR-ATR spectrum of the TiO_2/Fe_2O_3 sample has characteristic bands of absorption of TiO_2; at values lower than 800 cm^{-1} the presence of an absorption broadband corresponding to the vibration of the Ti-O bond is observed, the absorption bands of the stretch and vibration of the O-H bond are presented in 3170 cm^{-1} and in 1630 cm^{-1}, both bands being associated with the hydroxylated surface of the TiO_2/Fe_2O_3 sample.

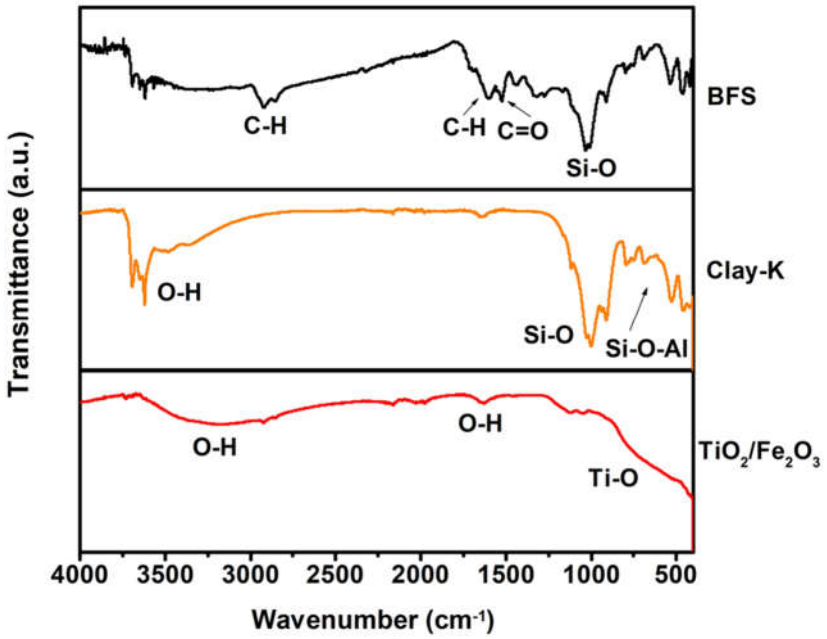

Figure 3. FTIR-ATR spectra of BFS, Clay-K, and TiO_2/Fe_2O_3 samples.

Figure 4a presents the diffractograms of the BFS, and Clay-K samples. The diffractograms of both samples show the characteristic diffraction peaks of SiO_2 in the crystalline form of quartz (PDF # 46-1045) and the characteristic diffraction pattern of kaolinite clay (PDF # 14-0164). Additionally, in the diffractogram of the BFS sample the presence of diffraction peaks that correspond to carbon graphite (C) is observed (PDF # 26-1079).

On the other hand, the diffractogram of the Sample TiO_2/Fe_2O_3 presents the diffraction peaks characteristic of the TiO_2 phase anatase (PDF # 21-1272) and of Fe_2O_3 hematite phase (PDF # 33-0664) (Figure 3b); the diffraction peak of the plane (101) of the anatase presents a slight displacement to higher degrees, possibly due to a small change in the volume of the cell; this can also be associated with the formation of the TiO_2/Fe_2O_3 composite.

Preprints (www.preprints.org) | NOT PEER-REVIEWED | Posted: 11 October 2022 doi:10.20944/preprints202210.0133.v1

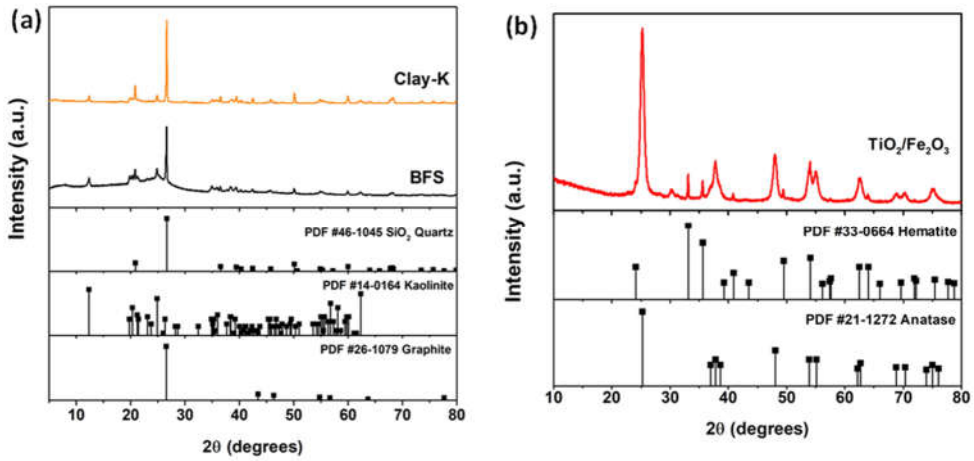

Figure 4. X-ray diffractograms of (a) BFS and Clay-K samples, and of (b) TiO_2/Fe_2O_3 sample. Diffraction patterns of quartz (PDF # 46-1045), (kaolinite (PDF # 14-0164), graphite (PDF # 26-1079), anatase (PDF 21-1272), and hematite (PDF 33-0664) are included.

Figure 5 shows the absorption spectra of the three samples; it is observed that the maximum absorption peaks of the TiO_2/Fe_2O_3 composite are in the UV region (326 nm) and visible region (520 nm) indicating that it can be excited with UV and visible light. In general, in this figure, it can be seen that both the Clay-K and BFS samples, as well as the TiO_2/Fe_2O_3 composite absorb light in over a wide region of the electromagnetic spectrum, from 200 nm to 1000 nm, so that UV, visible, and near infrared light can be used to photoactivate them.

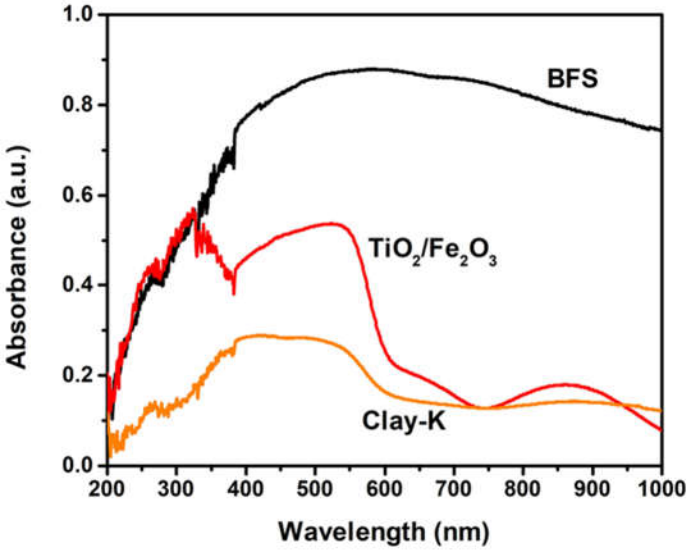

Figure 5. Absorption spectra of Clay-K, BFS, and TiO_2/Fe_2O_3 materials.

3.2. Removal of cyanide by adsorption and photocatalysis.

3.2.1. Cyanide adsorption

Figure 6 presents the cyanide adsorption values for each sample investigated, at initial NaCN concentrations of 250 mg/L and 750 mg/L. For an initial NaCN concentration of 250 ppm, with the use of the TiO_2/Fe_2O_3 sample and Clay-K, adsorption values of 46.5% (174.37 mg/g) and 50% (187.50 mg/g) were obtained. It is clear that cyanide adsorption is relatively low with the BFS sample, since only 36% (135 mg/g) was obtained, at an initial concentration of 750 mg/L NaCN.

Preprints (www.preprints.org) | NOT PEER-REVIEWED | Posted: 11 October 2022 doi:10.20944/preprints202210.0133.v1

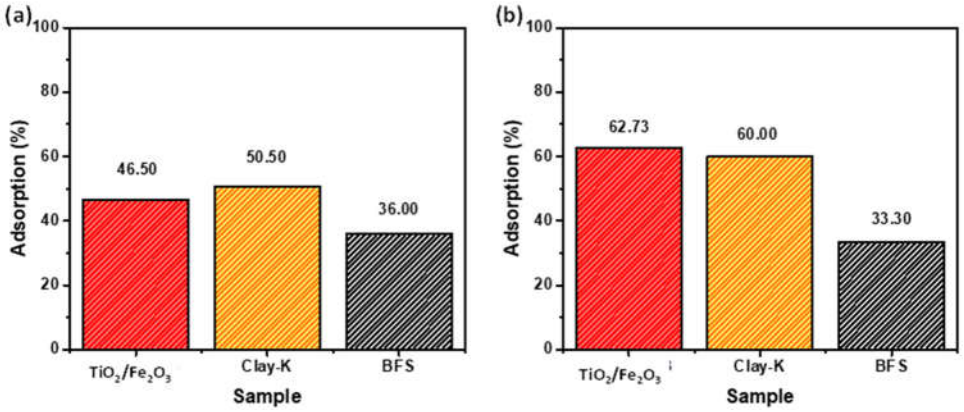

Figure 6. Percentage of cyanide adsorption in TiO_2/Fe_2O_3, Clay-K, and BFS materials, at initial concentrations of (a) 250 mg/L and (b) 750 mg/L NaCN. Adsorption time of 2 hours.

By increasing initial concentration of NaCN from 250 ppm to 750 mg/L, it can be seen that at a higher concentration, Clay-K sample adsorbs 60% (225 mg/g), surpassing the BFS sample that presents only 33.30% (124.87 mg/g), whereas up to 62.73% (219.55 mg/g) adsorption is obtained with the TiO_2/Fe_2O_3 sample. Clay-K and TiO_2/Fe_2O_3 samples adsorb approximately twice as much cyanide compared to the BFS sample, which is due to their low specific surface area (5.69 m^2/g) compared to that of the other two materials, being 66.59 m^2/g and 14.93 m^2/g for the TiO_2/Fe_2O_3 and Clay-K samples, respectively. It is worth mentioning that the amount of cyanide removed from the aqueous solution by the three adsorbent materials is higher than that reported by Behnamfard et al., who investigated the removal of free cyanide in aqueous solutions by adsorption, using kaolin. They obtained adsorptions of 2.5, 3, and 8 mg/g using crude, calcined and kaolin treated with sulfuric acid, respectively [9].

The results of cyanide adsorption in the three materials as a function of time, at the initial NaCN concentration of 750 ppm, are shown in Figure 7; it is observed that within 15 minutes of being in contact with Clay-K and TiO_2/Fe_2O_3 materials into cyanide solution, 40% adsorption is reached, while the BFS material only adsorbs 4.6% cyanide. At 120 minutes this same sample only adsorbs 38.76%, whereas Clay-K and TiO_2/Fe_2O_3 samples adsorb up to 63%.

Mathematical models of first and pseudo-second order were used to configure the adsorption kinetics, being the pseudo-second order the one with the best correlation (Figure 8 and Table 2), as indicated by the values of R^2 equal to 0.9692, 0.9529, and 0.9845, for the kinetics of cyanide adsorption in the TiO_2/Fe_2O_3, Clay-K, and BFS samples, respectively. The values of the apparent velocity constant of pseudo second order, K_2, are also listed in Table 2; the constant rate of cyanide adsorption in BFS material was lower than in the other two materials.

Preprints (www.preprints.org) | NOT PEER-REVIEWED | Posted: 11 October 2022 doi:10.20944/preprints202210.0133.v1

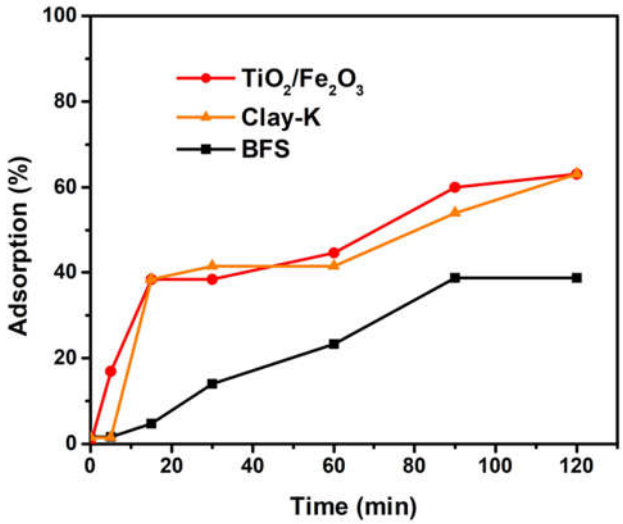

Figure 7. Cyanide adsorption kinetics in TiO_2/Fe_2O_3, Clay-K, and BFS samples.

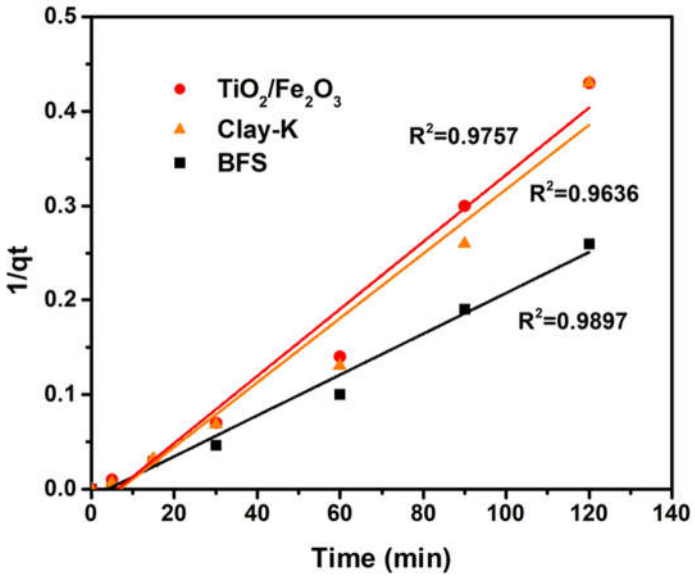

Figure 8. Modeling of cyanide adsorption kinetics in TiO_2/Fe_2O_3, Clay-K, and BFS samples. Pseudo second order model.

Table 2. Adsorption kinetics constants of pseudo second order model and R square constant.

Sample	K_2	R^2
TiO_2/Fe_2O_3	$3.55x10^{-3}$	0.9692
Clay-K	$3.41\ x10^{-3}$	0.9529
BFS	$2.16\ x10^{-3}$	0.9845

3.2.2. Cyanide photodegradation

The results of the ultraviolet (UV) light photodegradation tests, performed at an initial NaCN concentration of 750 ppm (Figure 9), indicate that using Clay-K and BFS as catalysts for cyanide degradation, higher percentages of degradation are achieved, obtaining 96.44% and 92.66%, respectively. The high percentages of cyanide photodegradation with the Clay-K and BFS indicate that these two catalysts are excited under UV irradiation efficiently, generating electron-hole pairs without recombining, to give rise to the formation of oxidizing species, which react with cyanide oxidizing it. On the other hand, the TiO_2/Fe_2O_3 catalyst photodegrades cyanide by 61.94%, which may be due to the fact that it absorbs photons in a smaller proportion than the other two materials in this region (see

Preprints (www.preprints.org) | NOT PEER-REVIEWED | Posted: 11 October 2022 doi:10.20944/preprints202210.0133.v1

Figure 5), or that there is electron-hole recombination. Figure 8 includes the photolysis of a cyanide solution of 750 mg / L, irradiated with UV light for 2 h, obtaining a 2.60% photodegradation.

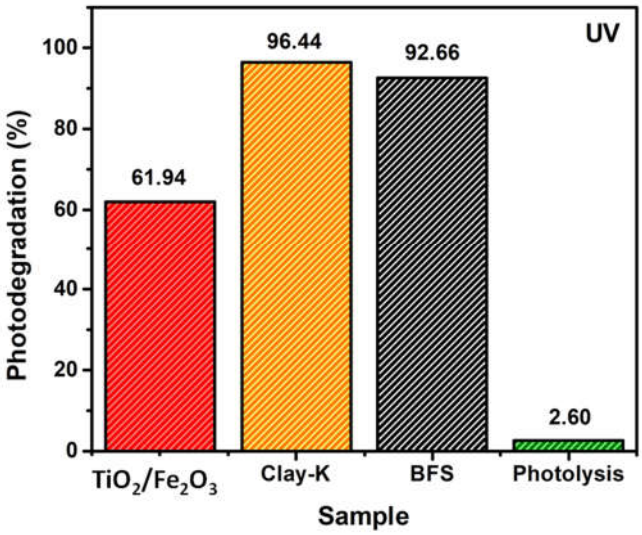

Figure 9. Percentages of cyanide photodegradation with Clay-K, BFS, and Fe_2O_3/TiO_2 materials, using UV irradiation for 2 h. Initial concentration of NaCN of 750 mg/L.

On the other hand, using visible light as an excitation source (Figure 10), TiO_2/Fe_2O_3 material has a higher percentage of degradation (74.11%) compared to that obtained with UV irradiation (61.94%). In contrast, the BFS and Clay-K materials photodegraded in a smaller percentage to cyanide, obtaining values of 74.40% and 68.33%; compared to the results obtained using irradiation with UV light, these two materials have about 30% less catalytic action under irradiation with visible light. These results indicate that the TiO_2/Fe_2O_3 material can be used as a catalyst for cyanide photo-oxidation under visible irradiation. This same Figure 10 includes the photolysis of a cyanide solution of 750 mg/L, irradiated with visible light for 2 h, obtaining a 2.73% of photodegradation.

Preprints (www.preprints.org) | NOT PEER-REVIEWED | Posted: 11 October 2022 doi:10.20944/preprints202210.0133.v1

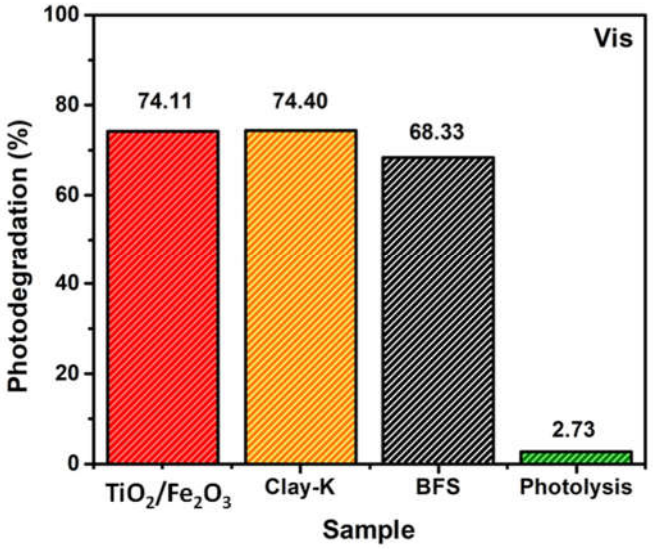

Figure 10. Percentages of cyanide photodegradation with Clay-K, BFS, and Fe_2O_3/TiO_2 materials, using irradiation with visible light for 2 h. Initial concentration of NaCN of 750 mg/L.

Additional, Figure 11 shows the exposure to natural solar irradiation from the above samples, for example, after exposure to UV or visible radiation, further potentiated the percentage of cyanide degradation with each material. When cyanide is exposed to irradiation with UV light plus natural sunlight, the percentage of cyanide degradation increased substantially with the TiO_2/Fe_2O_3 sample, obtaining a 98.66%. This figure also includes the photolysis of a cyanide solution of 750 mg / L, irradiated with UV and natural sunlight for 2 h, obtaining a 4.13% photodegradation.

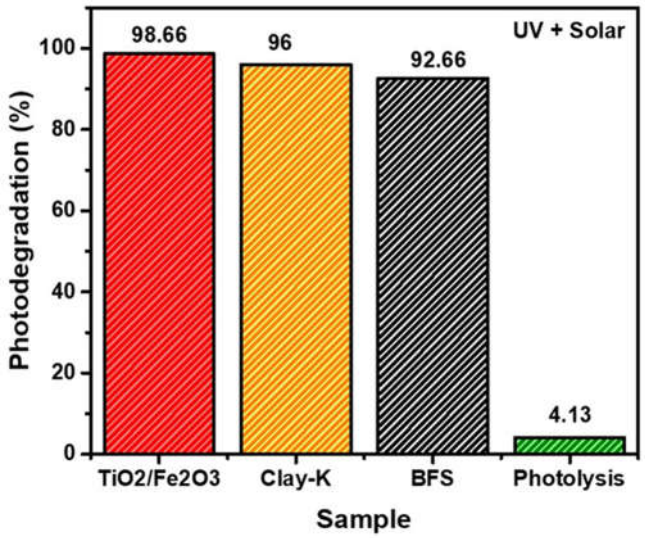

Figure 11. Percentages of cyanide photodegradation with Clay-K, BFS, and Fe_2O_3/TiO_2 materials, using UV and solar irradiation for 2 h. Initial concentration of NaCN of 750 mg/L.

The results obtained with visible radiation plus solar irradiation are shown in Figure 12. In this case, the cyanide photodegradation values with the three materials were 98.66%, 98.33%, and 98.66% with the materials TiO_2/Fe_2O_3, Clay-K, and BFS, respectively. This indicates that natural sunlight, composed of different types of radiation (visible, UV, and infrared) allows to generate different levels of excitation in the materials that contribute to the oxidation of cyanide. All three materials are highly efficient to photodegrading

Preprints (www.preprints.org) | NOT PEER-REVIEWED | Posted: 11 October 2022 doi:10.20944/preprints202210.0133.v1

cyanide under this irradiation scheme. This same figure includes the photolysis of a cyanide solution of 750 mg/L, irradiated with visible and natural sunlight for 2 h, obtaining a 6.9% photodegradation.

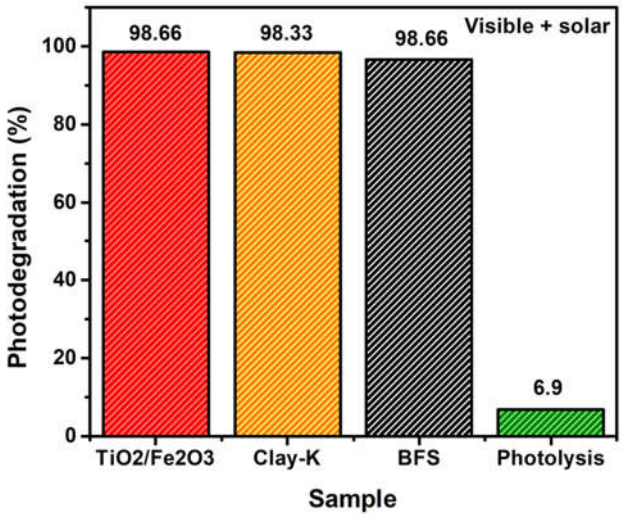

Figure 12. Percentages of cyanide photodegradation with Clay-K, BFS, and Fe_2O_3/TiO_2 materials, using visible and solar irradiation for 2 h. Initial concentration of NaCN of 750 mg/L.

Cyanide photodegradation kinetics were performed with the three materials, irradiating with natural sunlight a 750 ppm NaCN solution, over a period of 2 hours; previously, the suspensions were brought to the adsorption balance under absence of irradiation conditions. The results obtained are shown in Figure 13 (a) and (b), at solar irradiance values from 400 to 600 W/m² and from 600 to 800 W/m², respectively. As shown in Figure 12(b), the most efficient material to remove cyanide, using a solar irradiation range of 600 to 800 Wh/m², was the BFS sample, although the adsorption of cyanide was 33.30%; the total removal obtained is 97% in two hours of irradiation and 87% in just 30 minutes. On the other hand, with the TiO_2/Fe_2O_3 sample, which has greater cyanide adsorption than the BFS sample (62.73%), it removes less cyanide by photodegradation, even so, the amount of total cyanide removed with this material is not despicable, reaching up to 92.66% in two hours of irradiation and 80% in just 30 minutes of natural sunlight irradiation. In contrast, the Clay-K sample allows photodegradation up to 84.33% in two hours.

Figure 13 (a) presents the photodegradation results obtained by subjecting the cyanide-catalyst suspensions with a solar irradiance of 400 to 600 W/m² for two hours. At two hours of irradiation, the samples of TiO_2/Fe_2O_3 and Clay-K allow 84% and 82% of cyanide photodegradation, respectively, while the BFS sample photodegrades 72%. Comparing these results with those obtained with greater irradiation, it can be said that the greater the irradiation the photocatalytic activity of the three catalysts increases and that the photocatalytic activity of the Residue is more dependent on the intensity of irradiation than Clay-K and TiO_2/Fe_2O_3 samples. As for the effect of solar irradiation time on cyanide photodegradation with the three catalysts, and for both solar irradiation ranges, it is observed that the photodegradation rate is considerably higher in the first 30 minutes; even more, after this time, photodegradation continues to increase, but at a lower rate, meaning that it is less dependent on irradiation time. Eskandari et al. has reported that the longer the irradiation time the system has, the more reaction time there will be between the photocatalyst and cyanide, achieving a greater photodegradation of contaminants [27].

Preprints (www.preprints.org) | NOT PEER-REVIEWED | Posted: 11 October 2022 doi:10.20944/preprints202210.0133.v1

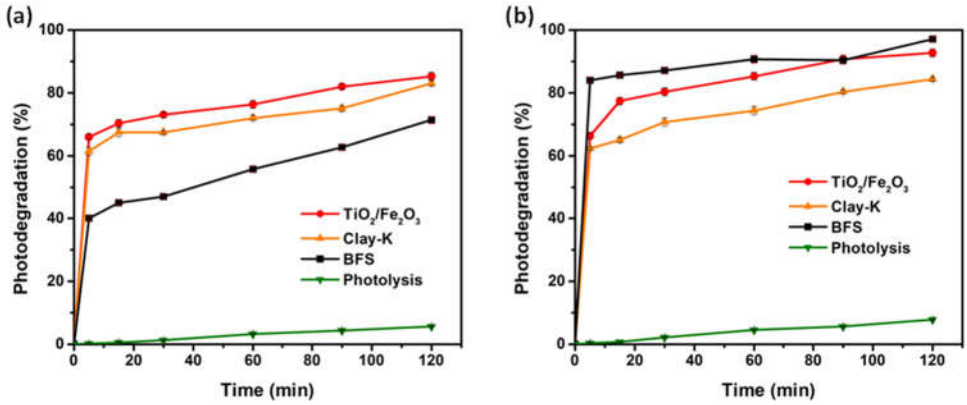

Figure 13. Cyanide degradation kinetics: (a) 400 – 600 Wh/m² and (b) 600 – 800 Wh/m². Effect of solar irradiance; 2 g/L catalyst.

Chiang and Amal states that cyanide rate of degradation is a function of the concentration of the catalyst, due to the volumetric absorption of photons and if the optimal value of the catalyst is exceeded, the percentages of degradation decrease due to the increased opacity in the solution and there is a greater scattering of light [20]. Otherwise, Pavas et al. reported that the concentration of the catalyst does not influence degradation, rather that its characteristics are what make this possible, having a high surface area distribution of uniform size and absence of internal porosity [21].

Eskandari et al. indicated that the higher the initial concentration of cyanide, the lower the efficiency of degradation; this is because there is a higher content of cyanide on the active surface of the catalyst, so the photons do not fully penetrate the photocatalyst, which decreases the generation of oxidizing species, because there is no direct reaction between the cyanide molecules and the photonic cavities [27].

In contrast, it is well known that the pH of the solution affects the surface load of adsorbent and catalytic materials, so it is recommended to work at a pH different from that of the zero charge point or the isoelectric point, so that these remain stable, that is, well dispersed in the solution to be treated; for TiO_2, the isoelectric point occurs at pH 7. Chiang et al. states that the surface of TiO_2 adsorbs and interacts only with cyanide under alkaline conditions, this confirmed by a change in its zeta potential [20].

At a pH below 9.2 cyanide dissociates and forms HCN. At pH between 9.5 and 12 the photocatalytic degradation is more favorable for cyanide, at pH 9.5 the percentage of degradation is higher. This is consistent with Yngard et al. which concludes that at pH greater than 11 the velocity constant decreases, this using Fe(VI) as a catalyst [26]. Compared to high pH above 12, where an unfavorable adsorption of CN^- ions occurs on the negatively charged surface of TiO_2.

Considering and comparing the results of adsorption and photodegradation obtained in this work at pH 11, with what is reported in the literature cited above, and considering that the zeta potential values of the Samples TiO_2/Fe_2O_3, Clay-K and BFS at this pH value is negative, that is, its surface is negatively charged, it is proposed that the adsorption of the cyanide anion is not governed by interactions of electrostatic attraction, but by the very possible formation of complexes by coordinated covalent bonds, followed by photooxidation from the surface of the oxides, when the oxidizing species are generated when the aqueous suspensions containing the catalyst particles are exposed to different light sources. In relation to the products obtained from the degradation of cyanide, Chiang et al. (2003), concludes that the oxidation of cyanate was insignificant, since the concentration of nitrates was almost undetectable, with cyanate being the only species obtained from the oxidation of cyanide. Agreeing with Yngard et al. that the conversion of cyanide was complete to cyanate [26].

 doi:10.20944/preprints202210.0133.v1

4. Conclusions

The analysis of the results obtained allows us to conclude the following:

4.1. Cyanide adsorption

Clay-K and TiO_2/Fe_2O_3 samples, using an initial NaCN concentration of 750 ppm, adsorb approximately twice as much cyanide (67.73%; 253.98 mg/g) compared to the BFS sample, which only adsorbs 33.3% (124.87 mg/g). This is due to their smaller specific surface area (5.69 m^2/g) compared to that of the other two materials. The first and pseudo-second order mathematical models were used to model the kinetics of cyanide adsorption, with the pseudo-second order being the one with the best correlation with the experimental data.

4.2. Cyanide photodegradation

Under irradiation with UV light, Clay-K and BFS samples act as excellent catalysts for cyanide photodegradation, values of 96.44% and 92.66% were obtained, respectively. On the other hand, the highest percentage of cyanide photodegradation, using UV irradiation plus natural sunlight, was obtained with the TiO_2/Fe_2O_3 sample, with 98.66% degradation.

The most efficient catalytic material to photodegrade cyanide under irradiation with natural sunlight, with an irradiance range of 600 to 800 W/m^2, is the BFS sample, reaching up to 97% (363.75 mg/g) cyanide removal in two hours of irradiation and 87% (326.25 mg/g) in just 30 minutes.

Author Contributions: Conceptualization, Carrillo-Pedroza, F. and Sanchez-Castillo, M.; Methodology, Martinez-Luevanos, A., M.; Validation, Martinez-Luevanos, A., Carrillo-Pedroza, F. and Amaro-Medina, B.; Formal Analysis, Martinez-Luevanos, A. and Soria-Aguilar, M.; Investigation, Amaro-Medina, B.; Data Curation, Carrillo-Pedroza, F.; Writing – Original Draft Preparation, Amaro-Medina, B. and Martinez-Luevanos, A.; Writing – Review & Editing, Estrada-Flores, S., and Soria-Aguilar, M.; Funding Acquisition and Technical Project Manager, Carrillo-Pedroza, F.R.

Funding: This research was funded by Consejo Nacional de Ciencia y Tecnología (Spanish for National Council of Science and Technology; abbreviated CONACYT), grant number A1-S-15832.

Acknowledgments: Authors appreciate the support of CONACYT for the development of this project. BMAM appreciates the scholarship granted by CONACYT for her postgraduate studies.

Conflicts of Interest: The authors declare no conflict of interest.

References

1. Medina, D.; Anderson, C. A review of the cyanidation treatment of copper-gold ores and concentrates. Metals, 2020, 10, 897.
2. Vargas, C.; Navarro, P.; Araya, E.; Pavez, F.; Alguacil, F. (2006). Recovery of gold from solutions with ammonia and thiosulfate using activated carbon. Rev. de Metal., 2006, 42, 3, 222–233.
3. Kalombo, J.; Simonsen, H.; Ndlovu, S. Improving the gold leaching process of refractory ores using the Jetleach reactor. Miner. Eng., 2019, 134, 300-308.
4. Serquén, Y. Influence of ozone and copper on cyanide degradation of mining effluents. Bs. Thesis. Universidad Nacional Pedro Ruiz Gallo. Lambayeque, Peru, Completion March 2, 2020.
5. Lottermoser, B. (2003). Cyanidation wastes of gold-silver ores. In: Mine Wastes. Lottermoser, B. Ed.; Springer, Berlin, Heidelberg, 171-184.
6. U.S. EPA. IRIS Toxicological review of hydrogen cyanide and cyanide salts (Final Report). U.S. Environmental Protection Agency, Washington, DC, EPA/635/R-08/016F, 2010.
7. Rice, N.; Rauscher, N.; Langston, J.; Myers, T. Behavioral toxicity of sodium cyanide following oral ingestion in rats: Dose-dependent onset, severity, survival, and recovery. Food Chem Toxicol. 2018, 114, 145-154.
8. Maulana, I.; Takahashi, F. Cyanide removal study by raw and iron-modified synthetic zeolites in adsorption experiments. J. Water Process. Eng., 2018, 22, 80-86.
9. Behnamfard, A.; Chegni, K.; Alaei, R.; Veglio, F. The effect of thermal and acid treatment of kaolin on its ability for cyanide removal from aqueous solutions. Environ. Earth. Sci., 2019, 78, 408.
10. Nafaâ, A.; Lotfi, M. Removal of cyanide from aqueous solution using impregnated activated carbon. Chem. Eng. Process., 2002, 41,17-21.

11. Aliprandini, P.; Veiga, M.; Marshall, B.; Scarazzato, T.; Espinosa, D. Investigation of mercury cyanide adsorption from synthetic wastewater aqueous solution on granular activated carbon. J. Water Process. Eng., 2020, 34, 101154.
12. Noroozifar, M.; Khorasani-Motlagh, M.; Ahmadzadeh, P. Cyanide uptake from wastewater by modified natrolite zeolite-iron oxyhydroxide system: Application of isotherm and kinetic models. J. Hazard. Mater., 2009, 166, 2–3, 1060-1066
13. Pirmoradi, M.; Hashemian, S.; Shayesteh, M. Kinetics and thermodynamics of cyanide removal by ZnO@NiO nanocrystals. Trans. Nonferrous Met. Soc. China., 2017, 27, 6, 1394–1403.
14. Swantomo, D.; Faturrahman, I.; Basuki, K.; Wongsawaeng, D. Chitosan-polyacrylamide graft copolymers prepared with gamma irradiation for gold cyanide adsorption, Polym.-Plast. Technol. Mater., 2020, 59,12, 1284-1291
15. Moussavi, G.; Khosravi, R.; Omran, N. Development of an efficient catalyst from magnetite ore: Characterization and catalytic potential in the ozonation of wáter toxic contaminants. Appl. Catal. A-Gen., 2012, 445-446, 42-49.
16. Mondal, M.; Mukherjee, R.; Sinha, A.; Sarkar, S.; De, S. Removal of cyanide from steel plant effluent using coke breeze, a waste product of steel industry. J. Water Process. Eng., 2019, 28, 135-143.
17. Zhang, L.; Jaroniec, M. Fundamentals of adsorption for photocatalysis. Surface Science of Photocalalysis. Interface Sci. Technol., 2020, 31, 39-60.
18. Coronel, S.; Endara, D.; Lozada, A.B.; Manangón-Perugachi, L.E.; de la Torre, E. Photocatalytic study of cyanide oxidation using titanium dioxide (TiO2)-Activated carbon composites in a continuous flow photo-reactor. Catalysts, 2021, 11, 924.
19. Sivaraman, C.; Vijayalakshmi, S.; Leonard, E.; Sagadevan, S.; Jambulingam, R. Current developments in the effective removal of environmental pollutants through photocatalytic degradation using nanomaterials. Catalysts, 2022, 12, 544.
20. Chiang, K.; Amal, R. Tran, T. Photocatalytic oxidation of cyanide: Kinetic and mechanistic studies. J. Mol. Catal. A. Chem. 2003, 193, 285-297.
21. Pavas, E.; Camargo, P.; Castro, C.; Pineda, T. Oxidación fotocatalitica del cianuro. Pavas, E. Ed. Universidad Eafit, Medellin, Colombia, 2005, 1-55.
22. Quispe L.; Arteaga, M.; Cardenas, E.; Lopez, L.; Santelices, C.; Palenque, E.; Cabrera, S. (2011). Removal of cyanide by combined UV/H2O2/TiO2 system. Rev. Boliv. Quim., 2011, 28, 113-118.
23. Viña, J.; Fernandez, B.; Fernandez, M.; Ayala, J.; Ania, C. Photochemical degradation of cyanides and thiocyanates from an industrial wastewater. Molecules, 2019, 24, 1373.
24. Caicedo, D.; Schadach, I; Betancourt, L. Photocatalytic degradation of ferricyanide as synthetic gold mining wastewater using TiO2 assisted by H2O2. REM, Int. Eng. J., 2020, 73, 1, 99-107.
25. Seung-Monk, L.; Diwakar, T. Application of ferrate (VI) in the treatment of industrial wastes containing metal-complexed cyanides: A green treatment. J. Environ. Sci., 2009, 21, 10, 1347-1352.
26. Yngard, R.; Damrongsiri, S.; Osathaphan, K.; Sharma, V. Ferrate(VI) oxidation of zinc-cyanide complex. Chemosphere, 2007, 69, 5, 729-73.
27. Eskandari, P.; Farhadian, M.; Solaimany, A.; Jeon, B. Adsorption and photodegradation efficiency of TiO2/Fe2O3/PAC and TiO2/Fe2O3/Zeolite Nanophotocatalysts for the removal of cyanide. Ind. Eng. Chem. Res. 2019, 58, 5, 2099–2112.
28. Győrfi, K.; Vágvölgyi, V.; Zsirka, B.; Horváth, E.; Szilágyi, R.; Baán, K.; Balogh, S.; Kristóf, J. Kaolins of high iron-content as photocatalysts: Challenges of acidic surface modifications and mechanistic insights. Appl. Clay Sci., 2002, 195, 15, 105722.
29. Szczepanik, B. Photocatalytic degradation of organic contaminants over clay-TiO2 nanocomposites: A review. Appl. Clay Sci. 2017, 141, 227-239.
30. Estrada-Flores, S.; Martínez-Luévanos, A.; Perez-Berumen, C.; García-Cerda, L.; Flores-Guia, T. Relationship between morphology, porosity, and the photocatalytic activity of TiO2 obtained by sol–gel method assisted with ionic and nonionic surfactants, Bol. Soc. Esp. Ceram. Vidr., 2020, 59, Pages 209-218.